A Technique for Global Monitoring of Net Solar Irradiance at the Ocean Surface. Part I: Model

ROBERT FROUIN* AND BETH CHERTOCK**

Scripps Institution of Oceanography, University of California, San Diego, La Jolla, California

(Manuscript received 7 December 1990, in final form 25 November 1991)

ABSTRACT

An algorithm based on radiative transfer theory is presented to generate the first accurate, long-term (84-month) climatology of net surface solar irradiance over the global oceans from *Nimbus-7* earth radiation budget (ERB) wide-field-of-view planetary-albedo data. Net surface solar irradiance is computed as the difference between the top-of-atmosphere incident solar irradiance (known) and the sum of the solar irradiance reflected back to space by the earth–atmosphere system (observed) and the solar irradiance absorbed by atmospheric constituents (modeled). Apart from planetary albedo and sun zenith angle, the most important parameters governing net surface solar irradiance variability, the model input parameters (water vapor and ozone amounts, cloud absorptance, aerosol type, and surface visibility), are fixed at their climatological values. It is shown that the effects of clouds and clear-atmosphere constituents can be decoupled on a monthly time scale, which makes it possible to directly apply the algorithm with monthly averages of ERB planetary-albedo data. Compared theoretically with the algorithm of Gautier et al., the present algorithm yields higher solar irradiance values in clear and thin cloud conditions and lower values in thick cloud conditions. The agreement, however, remains within 10–20 W m^{-2}.

1. Introduction

The solar radiation penetrating the oceans is an important component of the air–sea heat balance, the other components being the longwave radiation and latent and sensible heat emitted to the atmosphere. It constitutes a major boundary forcing for the oceanic circulation and acts as a crucial parameter for determining meridional heat transport. Our current understanding, however, of the spatial and temporal variability of ocean surface solar irradiance is still inadequate for investigations of climate and global change.

On climatological scales, knowledge of ocean surface solar irradiance is based on empirical formulas that involve parameters measured routinely aboard ships. This dataset is large but unevenly distributed and is, in some instances, of questionable quality. The southern oceans, in particular, are critically undersampled, making it difficult to trust the solar irradiance values calculated for those areas.

Satellites, which are well adapted to observe clouds (the major variable altering surface solar irradiance), offer the opportunity to establish a long-term, global climatology of ocean surface solar irradiance. However, due to the cost and availability of global satellite datasets, as well as the computational burden that the application of current satellite algorithms entails, we still do not have a long time series of surface solar irradiance over the world oceans.

The satellite-based methods of estimating surface solar irradiance ordinarily relate the outgoing solar radiance (measured in the visible and near-infrared region of the electromagnetic spectrum) at satellite altitude to the radiative properties of the system and to the surface solar irradiance. The use of remotely sensed radiance data from satellites is especially well-suited to the task of surface solar irradiance estimation for two general reasons. First, most of the solar radiation reaching the surface originates from visible and near-infrared wavelengths (0.4–1.0 μm). Energy at wavelengths longer than 1.0 μm is almost totally absorbed by even the thinnest clouds, and energy at wavelengths shorter than 0.4 μm is largely lost due to molecular scattering and absorption by ozone. Second, clouds are the main modulator of the surface solar irradiance, and they often can be observed easily from space. A high (low) value of net solar flux at the surface is consistently accompanied by a low (high) value of cloud optical thickness, and, therefore, a low (high) value of reflected solar flux at satellite altitude. The radiance data, however, are difficult to work with (e.g., transformation of radiance into irradiance and narrowband

* California Space Institute.

** Present affiliation: NOAA Environmental Research Laboratories, Wave Propagation Laboratory, Boulder, CO 80303.

Corresponding author address: Dr. Robert Frouin, California Space Institute, Scripps Institution of Oceanography, University of California, San Diego, La Jolla, CA 92093-0221.

to broadband conversion), costly, and not always readily available.

Approaches for estimating surface radiative fluxes may be divided into two categories: statistical techniques and physical-model techniques. Statistical techniques (e.g., Hay and Hanson 1978; Tarpley 1979; Justus et al. 1986) estimate surface solar irradiance from satellite data with the use of empirical formulas. The formulas have been obtained by relating measurements of solar irradiance made at the surface with concurrent satellite measurements. In contrast, physical-model techniques (e.g., Ellis and Vonder Haar 1979; Gautier et al. 1980; Mošer and Raschke 1984; Pinker and Ewing 1985; Dedieu et al. 1987; Darnell et al. 1988) do not require any prior comparisons with surface measurements. Instead, satellite observations are used to estimate the input parameters of a numerical model that is based on radiative transfer theory.

A physical-model technique is used in this investigation to obtain the net surface solar irradiance from the solar irradiance at the top of the atmosphere by subtracting both the solar energy reflected by the ocean–atmosphere system and the solar energy absorbed by the atmosphere. This approach follows a suggestion by Ramanathan (1986), based on model simulations, that a simple linear relationship might exist between the net downward solar flux at the top of the atmosphere and at the surface. The solar-irradiance model is designed essentially to incorporate *Nimbus-7* satellite measurements of planetary albedo (fractional percentage of incident solar irradiance that is reflected by the planetary system back into space), which are used to determine monthly averages of reflected solar irradiance. Despite research advances in this area (e.g., Cess and Vulis 1989), climate investigators have not been able to monitor variations in surface solar irradiance over the world oceans, and the model presented in the following section provides this capability when applied to *Nimbus-7* earth radiation budget (ERB) wide-field-of-view planetary-albedo data (see Chertock 1989; Chertock et al. 1992).

2. Solar-irradiance model

The principle underlying the current approach may be stated very simply: the solar irradiance reflected back to space by the ocean–atmosphere system and the solar irradiance absorbed by atmospheric constituents are subtracted from the top-of-atmosphere (TOA) incident solar irradiance to obtain the net solar irradiance at the ocean surface. The TOA incident solar irradiance is a well-known quantity that may either be calculated according to the astronomical configuration (as is done in this case) or measured using satellite radiometers. The TOA reflected solar irradiance is also readily determined using satellite radiometers. However, the total amount of solar irradiance absorbed by atmospheric constituents is not available from direct measurements but must be computed using a rather complicated numerical model. The success of the method depends on the adequacy of this model, which is described in detail below.

The solar-irradiance model is formulated using plane-parallel theory and assuming the isotropy of radiance reflected by clouds and the surface. The most critical underlying assumption is that the effects of clouds can be decoupled from the effects of the clear atmosphere. The planetary atmosphere is modeled, therefore, as a clear-sky atmosphere positioned above an effective cloud layer; that is, the solar irradiance at the surface is modeled as the product of a clear-sky component and a vertically integrated cloud transmittance. The great strength of such a decoupled model is its simplicity. It is unnecessary to distinguish between clear and cloudy regions within a pixel, which is convenient when the pixel is large spatially, and this feature eliminates entirely the need for difficult and often arbitrary decisions about the cloudiness distribution.

The basic components of the model are depicted in Fig. 1. Under solar incidence angle θ, the incoming irradiance at the top of the atmosphere, $I_\infty \cos\theta$, is diminished by a factor $t_a(\theta)t_g(\theta)(1 - S_aA)^{-1}$ when it enters the cloud layer. In this expression, t_a is the diffuse atmospheric transmittance due to scattering by aerosols and molecules, t_g is the transmittance due to gaseous absorption, S_a is the spherical albedo (i.e., the relative fraction of reflected solar irradiance backscattered toward the surface, taking into account multiple reflections in various directions), and A is the albedo of the cloud-layer–surface system. The term $(1 - S_aA)$ represents photons that have been reflected by the cloud-layer–surface system and backscattered toward the cloud layer. As the irradiance, $I_\infty \cos\theta t_a(\theta)t_g(\theta)(1 - S_aA)^{-1}$, passes through the cloud layer and the surface, it is further reduced by a factor of $A + a$, where a is the cloud-layer absorption. The solar irradiance penetrating the ocean is then given by

$$I(\theta) = I_{\text{clear}}(\theta)(1 - A - a)(1 - S_aA)^{-1}, \quad (1)$$

where $I_{\text{clear}} = I_\infty \cos\theta t_a t_g$ is the solar irradiance that would reach the surface if the cloud layer and the surface were nonreflecting and nonabsorbing ($A = a = 0$).

In order to compute I, it is necessary to express A and a as functions of known quantities. This is achieved in two stages. First a is expressed as a function of A, and then A is related to A_{sat}, the satellite-measured planetary albedo (the percentage of TOA incident solar irradiance that is reflected back to space by the planetary system). Consider first the albedo of the cloud-layer–surface system A. Under the plane-parallel assumption it can be written formally as

$$A = NA'_c + (1 - N)A_s, \quad (2)$$

where N is the cloud fraction, A'_c is the cloud-albedo contribution to A (including multiple surface reflec-

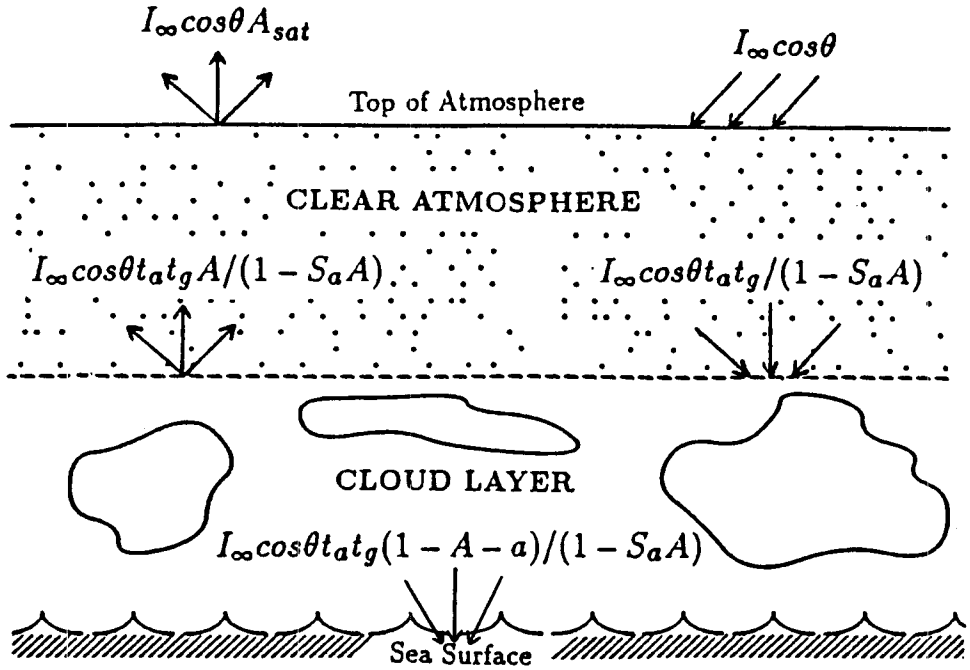

FIG. 1. Schematic diagram of the surface solar-irradiance model components.

tions), and A_s is the surface albedo. For a cloud of albedo A_c and absorption a_c,

$$A_c' = A_c + (1 - A_c - a_c)^2 A_s (1 - A_c A_s)^{-1}. \quad (3)$$

Using (3), the expression for A becomes

$$A \approx NA_c + A_s - 2NA_c A_s - 2Na_c A_s, \quad (4)$$

where $(1 - A_c A_s)^{-1}$ is approximated by $1 + A_c A_s$. Here second- and higher-order terms in A_c and A_s, as well as the term in $a_c A_c A_s$, have been neglected. Consider now the absorption of the cloud-layer–surface system, a. It can be written

$$a = Na_c' = N[a_c + (1 - A_c - a_c)a_c A_s (1 - A_c A_s)^{-1}], \quad (5)$$

where a_c' is the cloud-layer–surface absorption in overcast conditions. In clear-sky conditions ($N = 0$), $a = 0$. Developing the right-hand side of (5) and neglecting the second- and higher-order terms in A_c and A_s as well as the terms including a_c^2, one obtains

$$a \approx Na_c + Na_c A_s. \quad (6)$$

According to the theoretical calculations of Stephens et al. (1984), a_c can be expressed as a fraction of A_c, which yields

$$a \approx N\alpha A_c + N\alpha A_c A_s, \quad (7)$$

where α varies from 0.03 to 0.4 depending on θ and the cloud liquid water content. (As θ and the liquid water content increase, α decreases.) Incorporating this result into (4) yields

$$\alpha(A - A_s) \approx N\alpha A_c - 2N\alpha A_c A_s - 2N\alpha a_c A_s. \quad (8)$$

Since A_s is generally small (e.g., Payne 1972), the last term on the right-hand side of (7) and the last two terms on the right-hand side of (8) may be justifiably neglected. This simplification gives the following expression for the cloud-layer absorption:

$$a = \alpha(A - A_s). \quad (9)$$

Note that (1), (3), and (5) are only valid for monochromatic radiation, yet they are used to express broadband quantities. This is justified for (3) and (5), because A and a can be linearized with respect to A_s and/or A_c (since the value of A_s is small). For (1), however, the problem cannot be linearized, and therefore, it is assumed that the cloud-layer–surface albedo does not depend on wavelength. Since no information is given on the cloudiness distribution within a given satellite pixel, this assumption is appropriate. The approximation is reasonably accurate for cloudy conditions (since clouds are spectrally rather white) but not for clear-sky conditions. In clear-sky conditions, however, A reduces to A_s, and therefore, the resulting error in $I(\theta)$ is small, except for cases of large solar zenith angles.

With a thus related to A, the task becomes one of expressing A as a function of A_{sat}, the planetary albedo measured by the satellite. Since the reflectance of the cloud-layer–surface system is assumed Lambertian (A does not depend on the radiation geometry), A_{sat} can be modeled as

$$A_{sat}(\theta) = A_a(\theta) + AT_a(\theta)(1 - S_a A)^{-1}, \quad (10)$$

with

$$A_a(\theta) = \frac{1}{\pi} t_g(\theta) \int_0^{\pi/2} d\theta' \times \int_0^{2\pi} d\phi_r [r_a(\theta, \theta', \phi_r) t_g(\theta') \sin\theta' \cos\theta'] \quad (11)$$

$$T_a(\theta) = 2t_a(\theta) t_g(\theta) \int_0^{\pi/2} d\theta' [t_a(\theta') t_g(\theta') \sin\theta' \cos\theta'], \quad (12)$$

where θ' is the zenith angle characterizing the radiance emerging from the atmosphere, ϕ_r is the relative azimuth angle between the directions of emerging radiance and solar incidence, r_a is an intrinsic atmospheric reflectance (i.e., the contribution to A_{sat} due to photons that are backscattered by the atmosphere and return to space without ever reaching the cloud layer), and again t_g and t_a are the transmittances due to gaseous absorption and molecular and aerosol scattering, respectively. In (10), A_a represents the contribution to A_{sat} due to the backscattering of photons by the clear atmosphere, and $AT_a(1 - S_aA)^{-1}$ represents the contribution associated with photons that have sustained one or more reflections by the cloud layer.

A radiative transfer code, developed by Tanré et al. (1986) and based on Tanré et al. (1979), is used to compute r_a, t_g, and t_a. Referred to in the published literature as "5S" (simulation of the satellite signal in the solar spectrum), the radiative transfer code relates the reflected solar radiance measured by a satellite sensor in cloudless conditions to the radiative properties of the planetary system. The 5S code distinguishes between the contributions to the satellite-measured radiance due to distinct categories of scattering and absorption interactions. These contributions (which establish the values of r_a, t_a, and t_g) will now be discussed qualitatively.

The signal of reflected solar radiance that is measured by satellite sensors depends on the reflectance of the planetary surface, but it is also affected by atmospheric absorption (by gases and to a lesser extent by aerosols) and atmospheric scattering (by molecules and aerosols). If there were no intervening atmosphere, all of the incoming solar radiation would reach the surface, where a fraction would be absorbed and the rest would simply be reflected back to space. In fact, only a limited percentage of the photons reflected by the surface ever reach the satellite sensor (about 80% at 850 μm and about 50% at 450 μm), due to atmospheric absorption and scattering. Therefore, the target area viewed by the satellite is actually more reflecting than a simplistic interpretation of the signal would indicate, and so it is necessary to take absorption and scattering into account explicitly in the model.

Ozone (O_3), water vapor (H_2O), oxygen (O_2), and carbon dioxide (CO_2) are the main contributors to atmospheric absorption in the solar spectrum. Oxygen and carbon dioxide are quite uniformly mixed in the atmosphere at essentially constant concentrations for radiative purposes. In contrast, ozone and water vapor amounts vary significantly (both in space and over time) and therefore make a variable contribution to the satellite-measured reflected radiances. In the 5S code, atmospheric gaseous absorption is treated using the exponential band models of Goody (1964; water vapor) and Malkmus (1967; ozone, oxygen, and carbon dioxide). In each of these cases, the absorption lines are assumed to be randomly distributed over spectral intervals of width 20 cm^{-1}. Finally, the total gaseous transmissivity is computed as the product of the transmissivities due to the individual gases.

In general, gaseous absorption is not significant in the spectral bands of the satellite sensor channels. Therefore, gaseous absorption can be decoupled from the other processes, and is treated as simply a correction factor in the 5S code.

Aerosols and molecules primarily influence the satellite signal through scattering interactions. The scattering of photons by molecules or by aerosols is an elastic process that results in an instantaneous change in the directed photon path. Photons that are scattered numerous times may follow a relatively complicated path through the atmosphere before they exit back to space. The scattered photons must be accounted for in order to reconstruct a true measure of the surface reflectance. This reconstruction involves several distinct signal components, which are discussed in detail by Tanré et al. (1986).

The input parameters required by the code are the geometrical conditions; the vertical distributions of water vapor and ozone in the atmosphere, as well as total water vapor and ozone amounts; an aerosol model specifying maritime or continental background and aerosol concentration (parameterized as a function of visibility); and the ground reflectance (given as a function of wavelength). Our calculations are based on conditions of a 23-km visibility (United States 1962) standard atmosphere containing standard maritime aerosols (World Meteorological Organization 1983) and climatological values of water vapor and ozone amounts that vary with latitude and season (Table 1; McClatchey et al. 1971).

TABLE 1. Latitudinal and seasonal variations of the water vapor and ozone amounts input to the radiative transfer model.

Model	Water vapor amount (g cm^{-2})	Ozone amount (atm cm)
Tropical	4.12	0.25
Midlatitude summer	2.93	0.32
Midlatitude winter	0.85	0.40
Subarctic summer	2.10	0.35
Subarctic winter	0.42	0.48

The solar-irradiance model has been developed using reasoning involving spectral and directional quantities. We have argued, however, that the formalism is also valid for broadband quantities. Using (10) with broadband planetary-albedo data requires integration of the atmospheric functions A_a (11) and T_a (12) over wavelength. This is done by weight-averaging the functions with respect to the top-of-atmosphere spectral solar irradiance. Since the ERB planetary-albedo data (hereafter referred to as $\bar{A}_{\text{sat}}$) are in the form of monthly averages, the broadband A_a and T_a must also be averaged over time. For each month of the year, $\bar{A}_a$ and $\bar{T}_a$ are therefore computed as

$$\begin{pmatrix} \bar{A}_a \\ \bar{T}_a \end{pmatrix} = \frac{1}{M} \sum_{j=1}^{M} \frac{\int_{t_j^{\text{rise}}}^{t_j^{\text{set}}} dt \left\langle \begin{Bmatrix} A_a[\theta_j(t)] \\ T_a[\theta_j(t)] \end{Bmatrix} \cos[\theta_j(t)] \right\rangle}{\int_{t_j^{\text{rise}}}^{t_j^{\text{set}}} dt \{\cos[\theta_j(t)]\}}, \quad (13)$$

where j identifies the particular day of the month, t_j^{rise} and t_j^{set} are sunrise and sunset times, respectively, and M is the number of days in the month.

Figures 2 and 3 display the variation of $\bar{A}_a$ and $\bar{T}_a$, respectively, with latitude and month of the year. The function $\bar{A}_a$ takes greater values at high latitudes (in both the Northern and Southern hemispheres), with maximum values during winter. This reflects, to a large extent, the latitudinal and seasonal variations of the solar zenith angle. As θ varies, r_a and t_g in (11) vary in the same and opposite directions, respectively. The resulting effect of r_a on $\bar{A}_a$ generally dominates (increasing $\bar{A}_a$ with latitude), especially in the winter latitudes, but is somewhat compensated by that of t_g in the summer latitudes. For $\bar{T}_a$, the variations follow more closely the variation of the solar zenith angle, since both t_a and t_g in (12) decrease when θ increases. Using $\bar{A}_a$ and $\bar{T}_a$ with $\bar{A}_{\text{sat}}$ in (10) and solving for $\bar{A}$, the monthly

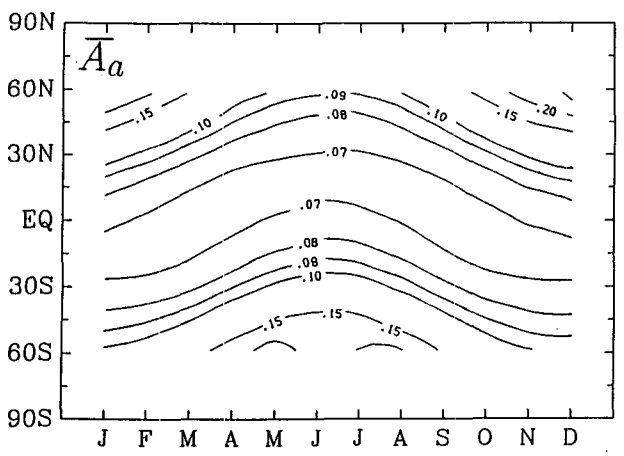

FIG. 2. Variation of $\bar{A}_a$, the monthly mean intrinsic atmospheric reflectance, as a function of latitude and time of year.

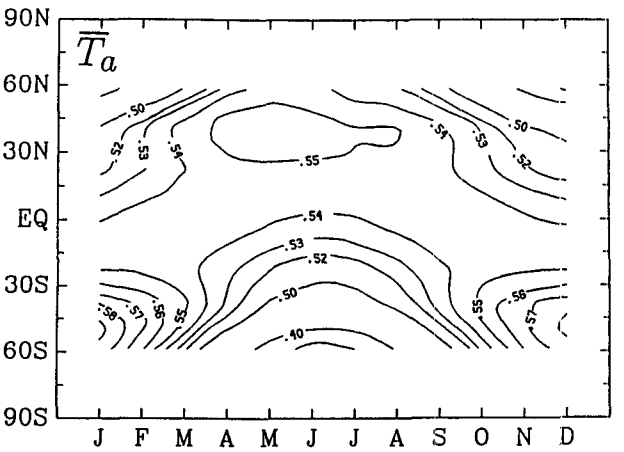

FIG. 3. Variation of $\bar{T}_a$, the monthly mean diffuse atmospheric transmittance, as a function of latitude and time of year.

averaged albedo of the cloud-layer–surface system then yields

$$\bar{A} = (\bar{A}_{\text{sat}} - \bar{A}_a)[\bar{T}_a + S_a(\bar{A}_{\text{sat}} - \bar{A}_a)]^{-1}. \quad (14)$$

For the 23-km-visibility atmosphere selected, S_a (weighted spectrally by the top-of-atmosphere solar irradiance) takes the value 0.11. Note that (14) is valid because A in (10) does not depend on θ, a basic assumption of the model.

Figure 4 shows the relationship between $\bar{A}$ and $\bar{A}_{\text{sat}}$ for July and latitudes of 40°S, 0°, and 40°N. As the

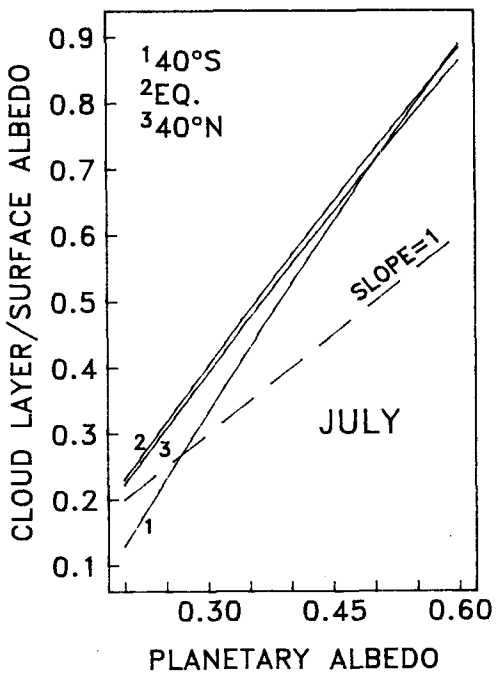

FIG. 4. Relationship between planetary albedo $\bar{A}_{\text{sat}}$ and cloud-layer–surface albedo A for July and latitudes of 40°S, 0°, and 40°N.

cloud-layer–surface albedo $\bar{A}$ increases, the planetary albedo $\bar{A}_{sat}$ increases, but at a slower rate. At the equator and 40°N, $\bar{A}$ becomes less than $\bar{A}_{sat}$ when $\bar{A}$ is less than 0.18, while at 40°S $\bar{A}$ becomes less than $\bar{A}_{sat}$ when $\bar{A}$ is less than 0.27. The relationship's nonlinearity is noticeable in Fig. 4, but remains small as expected [$T_a \gg S_a(\bar{A}_{sat} - \bar{A}_a)$].

As mentioned previously, α depends on θ and the cloud liquid water content. But taking α as a function of θ is not consistent with the assumption that A is constant with respect to radiation geometry. We can always assign, however, different values to $\bar{\alpha}$, the monthly averaged coefficient characterizing cloud absorption, according to latitude and month during the year. In view of the uncertainties in the theoretical values of α found in the published literature [models including that of Stephens et al. (1984) disagree with observations; for example, Foot (1988)] and since the cloud liquid water content or optical thickness must be specified to perform the computations (which introduces additional error), $\bar{\alpha}$ is defined as

$$\bar{\alpha} = \frac{1}{M}\sum_{j=1}^{M} \frac{\int_{t_j^{rise}}^{t_j^{set}} dt\{\alpha[\theta_j(t)]\}}{t_j^{set} - t_j^{rise}}. \quad (15)$$

This quantity, computed for a cloud optical thickness of 10 using the model of Stephens et al. (1984), is shown in Fig. 5 as a function of latitude and month of the year. Since α decreases as θ increases, in general maximum values of $\bar{\alpha}$ are obtained in the tropical and equatorial regions, as well as farther toward the poles during the associated summer months. Although $\bar{\alpha}$ remains small, one should still emphasize the arbitrariness of the values displayed in Fig. 5. Our assumptions are only warranted by the quality of the resulting predictions. Note, furthermore, that α can also be viewed as a tuning parameter that corrects for uncertainties in sensor calibration that change A_{sat} and, hence, A artificially.

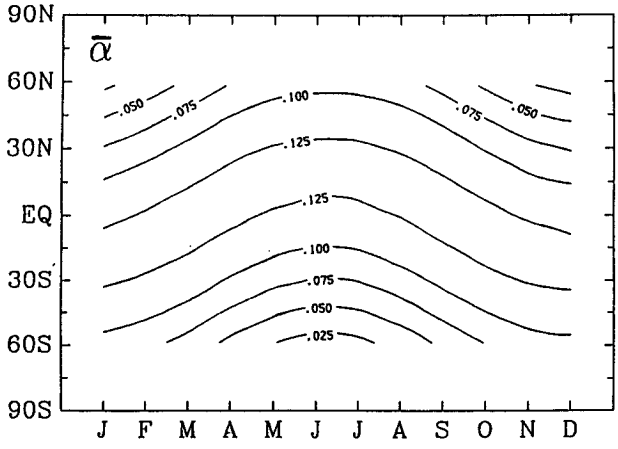

FIG. 5. Variation of $\bar{\alpha}$, the monthly mean cloud absorption coefficient, as a function of latitude and time of year.

The remaining task is one of expressing $I_{clear}(\theta)$ in (1) as a function of known parameters. Applying the formula developed by Frouin et al. (1989),

$$I_{clear}(\theta) = I_\infty \cos\theta \exp[-(f/V + g)/\cos\theta] \times \exp[-0.041(U_0/\cos\theta)^{0.57}] \times \exp[-0.102(U_w/\cos\theta)^{0.29}], \quad (16)$$

where V is visibility (km), U_0 is ozone amount (atm cm), U_w is water vapor amount (g cm^{-2}), and f and g are coefficients that depend on aerosol type. The first exponential in (16) represents the effects due to scattering by molecules and aerosols and also those due to absorption by aerosols. The second and third exponentials represent the effects due to absorption by ozone and water vapor, respectively. For the standard maritime atmosphere selected, $f = 0.359$ and $g = 0.059$. The formula (16) has been verified (Frouin et al. 1989) in midlatitude and tropical regions and shown to be accurate to ±6.5% (rms) on an hourly time scale.

Finally, since $\bar{A}_{sat}$ represents monthly averaged measurements, the expression for $I_{clear}(\theta)$ given in (16) must be converted into the corresponding monthly mean parameter $\bar{I}_{clear}$. Therefore, the monthly mean surface solar irradiance $\bar{I}$ is computed as

$$\bar{I} = \bar{I}_{clear}(1 - \bar{A} - \bar{a})(1 - S_a\bar{A})^{-1}, \quad (17)$$

with

$$\bar{a} = \bar{\alpha}(\bar{A} - \bar{A}_s) \quad (18)$$

and

$$\bar{I}_{clear} = \frac{1}{M}\sum_{j=1}^{M} \frac{\int_{t_j^{rise}}^{t_j^{set}} dt\{I_{clear}[\theta_j(t)]\}}{\Delta t}, \quad (19)$$

where $\bar{A}_s$ is the monthly mean surface albedo, taken to be equal to 0.06, and Δt is the length of the day (24 h). Figure 6 displays the variation of $\bar{I}_{clear}$ with latitude and month of the year, which corresponds closely to the known picture of surface solar irradiance under clear skies.

Figure 7 shows net surface solar irradiance as a function of planetary albedo for the month of July and latitudes of 40°S, 0°, and 40°N. Although (17) and (14) are not linear with respect to $\bar{A}$ and $\bar{A}_{sat}$, respectively, $\bar{I}$ is reduced almost linearly as $\bar{A}_{sat}$ increases, the slope of variation depending essentially on $\bar{I}_{clear}$. Thus, the slope is more negative at 40°N than at the equator and at 40°S. In order to explain the linearity of the relationship between $\bar{I}$ and $\bar{A}_{sat}$, write $\bar{I}$ as

$$\bar{I} \approx \bar{I}_{clear}\left\{1 - \frac{(\bar{A}_{sat} - \bar{A}_a)}{\bar{T}_a}\left[1 - \frac{S_a}{\bar{T}_a}(\bar{A}_{sat} - \bar{A}_a)\right] \times (1 - \bar{\alpha}) + \bar{\alpha}\bar{A}_s\right\}\left[1 + \frac{S_a}{\bar{T}_a}(\bar{A}_{sat} - \bar{A}_a)\right], \quad (20)$$

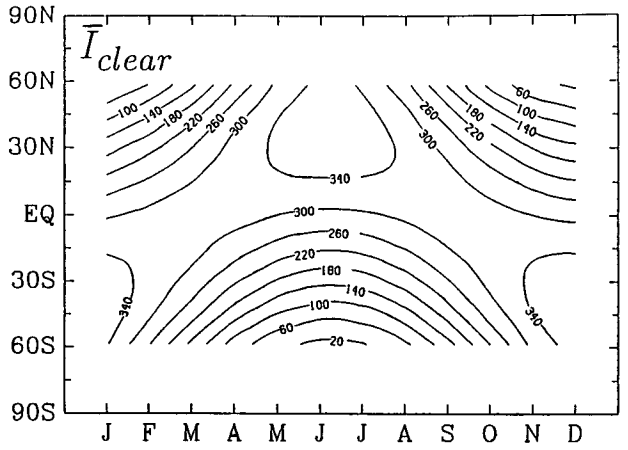

FIG. 6. Variation of $\bar{I}_{clear}$, the monthly mean solar irradiance that would reach the surface if the cloud layer were nonreflecting and nonabsorbing, as a function of latitude and time of year. The contour interval is 40 W m^{-2}.

where we have justifiably approximated

$$[\bar{T}_a + S_a(\bar{A}_{sat} - \bar{A}_a)]^{-1}$$

$$\text{by} \quad \left(\frac{1}{\bar{T}_a}\right)[1 - S_a(\bar{A}_{sat} - \bar{A}_a)/\bar{T}_a]$$

and

$$\{1 - S_a(\bar{A}_{sat} - \bar{A}_a)/[\bar{T}_a + S_a(\bar{A}_{sat} - \bar{A}_a)]\}^{-1}$$

$$\text{by} \quad [1 + S_a(\bar{A}_{sat} - \bar{A}_a)/\bar{T}_a].$$

Developing the right-hand side of (20) leads to

$$\bar{I} \approx \bar{I}_{clear}\left[1 - \frac{(\bar{A}_{sat} - \bar{A}_a)}{\bar{T}_a}(1 - \bar{\alpha}) + \bar{\alpha}\bar{A}_s + \epsilon(\bar{A}_{sat})\right], \tag{21}$$

where $O(\epsilon) = 10^{-3}$. Since $O(\bar{A}_{sat}/\bar{T}_a) = 1$, $\bar{I}$ is practically linear in $\bar{A}_{sat}$. This further indicates that neglecting the contribution of photons backscattered by the atmosphere toward the cloud-layer–surface system in (14) and (17) (taking $S_a = 0$) will not change the model outputs significantly.

3. Comparison with the model of Gautier et al. (1980)

To assess theoretically the performance of the model described above, its predictions for typical atmospheric and surface conditions may be compared with those of a validated model. The model of Gautier et al. (1980) has been selected, which, although based on simplified radiative transfer theory, has been verified extensively over the oceans (e.g., Gautier 1981, 1988; Gautier and Katsaros 1984; Frouin et al. 1988; Bates and Gautier 1989) and has been shown to be accurate to within ±10% (rms) on a daily time scale. In addition, a comparison of operational models to compute surface solar irradiance (Raphael and Hay 1984) demonstrated the better performance of the Gautier et al. model. Furthermore, comparing theoretically our model results with those of the Gautier et al. model is all the more interesting since the two models are intercompared using actual satellite data as input by Chertock (1989) and Chertock et al. (1992).

In order for the comparison to be meaningful, one must know exactly how the input parameters of the two models correspond. Instantaneous Geostationary Operational Environmental Satellite (GOES) Visible–Infrared Spin Scan Radiometer (VISSR) bidirectional reflectance in the 0.5–0.9-μm channel is required in the Gautier et al. model, and monthly broadband planetary albedo is required in the present model. Instead of employing a sophisticated radiative transfer model to establish the relationship between instantaneous VISSR reflectance and broadband albedo for typical targets (clouds and surface), radiometric measurements made aboard a high-flying aircraft, the National Aeronautics and Space Administration (NASA) CV-990, during the Monsoon Experiment (MONEX) (Smith et al. 1981), are used. Although the aircraft flew over a limited region (Indian Ocean) during a limited time period (summer 1979), it acquired data in sufficiently varied atmospheric and surface conditions and radiation geometries to give a good idea of the discrepancies between the two model outputs. Table 2 summarizes the regression analysis performed by Smith et al. (1981) for thin cloud, thick cloud, and ocean cases. The relations between the broadband directional reflectance r_b and the *GOES-1* VISSR directional reflectance r_g were obtained from the CV-990

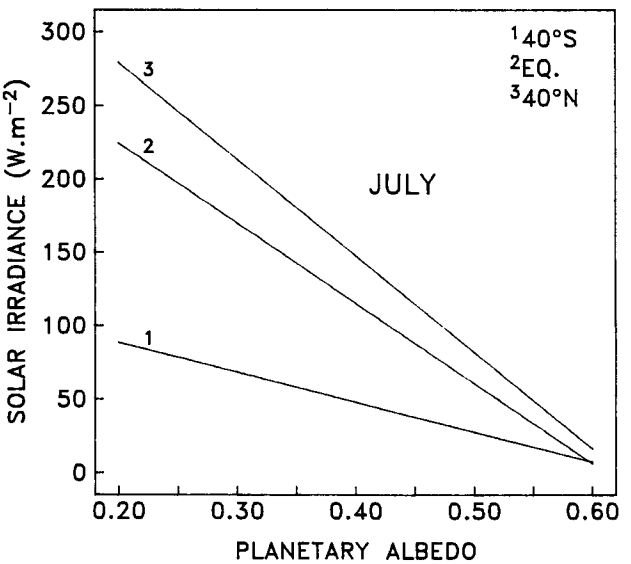

FIG. 7. Net surface solar irradiance $\bar{I}$ as a function of planetary albedo $\bar{A}_{sat}$ for July and latitudes of 40°S, 0°, and 40°N.

TABLE 2. Linear regression equations used to convert broadband albedo A^* into broadband directional reflectance r_b and *GOES*-1 VISSR directional reflectance r_g (after Smith et al. 1981).

Equation	Number of points	Standard error of estimate	Correlation coefficient	Condition
$A^* = 1.174 r_b$	91	0.023	.99	All†
$r_b = 0.749 r_g + 0.01747$	65	0.003	.99	Ocean
$r_b = 0.736 r_g + 0.02385$	55	0.007	.99	Thin cloud
$r_b = 0.600 r_g + 0.08849$	48	0.012	.99	Thick cloud

† Includes vegetation and desert.

multispectral radiometer (MSR) 0.3–4.0- and 0.5–0.9-μm (similar to the *GOES-1* VISSR solar channel) radiances. The relation between broadband angularly integrated albedo, A^* (equivalent to A_{sat}), and r_b was obtained from CV-990 MSR 0.3–4.0-μm radiances observed at small viewing zenith angles (<10°) and simultaneous 0.3–4.0-μm pyranometer measurements. For each of the Table 2 cases, the procedure to convert broadband albedo into *GOES-1* VISSR reflectance is as follows.

First, we have to define $A^*(\theta)$. This is done by expressing $A^*(\theta)$ as the product of a directional function and the albedo at $\theta = 0°$:

$$A^*(\theta) = \gamma(\theta) A^*(\theta = 0°), \qquad (22)$$

where $\gamma(\theta)$ is taken from Minnis and Harrison (1984) and $A^*(\theta = 0°)$ is fixed at 0.1, 0.2, and 0.4 for ocean, thin cloud, and thick cloud, respectively. Table 3 gives $\gamma(\theta)$ and Fig. 8 displays $A^*(\theta)$ for the three cases considered. Note that the same directional model is selected for thin and thick clouds.

The second step is to transform broadband albedo into broadband reflectance, by applying the relation $r_b = A^*/1.174$ (see Table 2). This relation was established for a wide range of solar zenith angles but for small viewing zenith angles. Therefore, our choice of VISSR viewing geometry is made accordingly (see below).

The final step gives access to *GOES-1* VISSR reflectance from broadband reflectance using the appropriate formulas of Table 2. Figure 8 displays the resulting *GOES-1* VISSR reflectance versus sun zenith angle for the three cases considered. Notice in this figure that $A^*(\theta)$ and $r_g(\theta)$ are similar for ocean and thin cloud but substantially different ($r_g > A^*$) for thick cloud, especially at large solar zenith angles. In view of the standard errors of regression given in Table 2, if A^* is fixed (as done above), the resulting error in r_g is within ±3%.

The Gautier et al. model was run with $r_g(\theta)$ as defined in Fig. 8 to produce monthly averaged net surface solar irradiance at latitudes of 0° and 31.5°N. In the calculations, the viewing zenith and azimuth angles were 0° and undefined, respectively (at the equator), and 36.7° and 180°, respectively (at 31.5°N), where the azimuth angle is defined with respect to the north. Other viewing geometries could have been selected, but they would not have changed the conclusions of the study. It was necessary, however, to keep the viewing zenith angles small enough for the relation between broadband albedo and broadband reflectance to be applicable. The value of 36.7° exceeds the condition of

TABLE 3. Directional function $\gamma(\theta)$ used to define broadband albedo $A^*(\theta)$ (after Minnis and Harrison 1984).

	$\gamma(\theta)$	
θ (°)	Ocean	Cloud
0	1.00	1.00
10	1.00	1.00
20	1.02	1.01
30	1.06	1.05
40	1.20	1.10
50	1.37	1.19
60	1.70	1.34
70	2.39	1.55
80	3.60	1.83

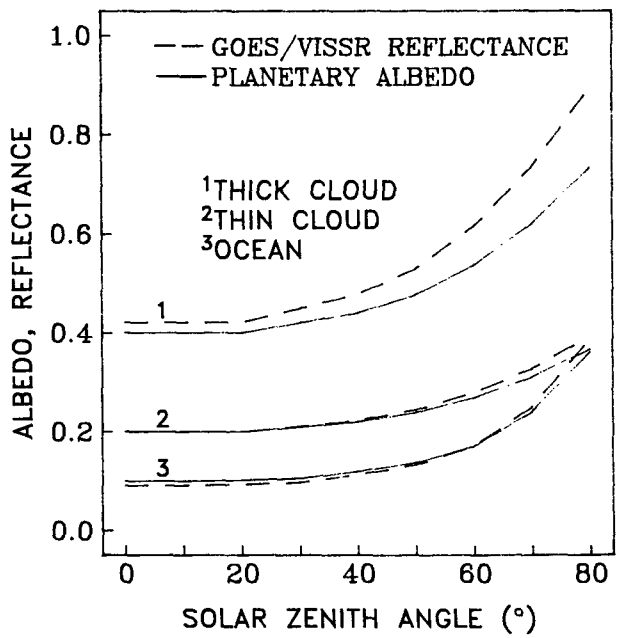

FIG. 8. Broadband planetary albedo and corresponding *GOES-1* VISSR reflectance (small viewing angles) for ocean, thin-cloud, and thick-cloud conditions.

small (i.e., <10°) viewing zenith angle, but the effects of viewing geometry for viewing zenith angles less than 40° are the same order of magnitude as those of solar geometry (see, e.g., Taylor and Stowe 1984), and the latter effects are neglected when using a unique relationship between r_b and A^* for all solar zenith angles.

The present model was run with monthly averaged planetary-albedo values computed from $A^*(\theta)$ given in Fig. 8 as

$$\bar{A}^* = \frac{1}{M}\sum_{j=1}^{M}\frac{\int_{t_j^{\text{rise}}}^{t_j^{\text{set}}} dt\{A^*(\theta)\cos[\theta_j(t)]\}}{\int_{t_j^{\text{rise}}}^{t_j^{\text{set}}} dt\{\cos[\theta_j(t)]\}}, \quad (23)$$

where t_j^{rise} and t_j^{set} are the sunrise and sunset times for day j of the month at the latitude under consideration and M is the number of days.

For both models, the same parameterization of net surface solar irradiance under clear skies, given in (16), was used. The clear atmosphere was assumed to contain maritime aerosols and climatological water vapor and ozone amounts and to have a 23-km visibility.

The results are presented in Fig. 9. In the case of ocean and thin cloud, our model yields higher net surface solar irradiance values than the Gautier et al. model. The differences range between 0 and 10 W m^{-2} in the ocean case, with maximum values at the equator all year long and at 31.5°N during summer. The same type of discrepancy is obtained for thin clouds, except that the differences are now higher, ranging from 10 to 20 W m^{-2}. In clear-sky conditions (ocean case), the differences are explained by our model providing $\bar{A} < 0.06$ instead of 0.06, the value used in the Gautier et al. model. Such $\bar{A}$ values might result partly from the accuracy of the atmospheric corrections on $\bar{A}_{\text{sat}}$ and partly from the values chosen for the atmospheric parameters, which probably correspond to $A^*(\theta = 0°) > 0.1$. Choosing $A^*(\theta = 0°) = 0.1$ in our ocean model, however, is consistent with the values reported by Rashke et al. (1973), Taylor and Stowe (1984), and others. In fact, when using the model with actual planetary-albedo data, one could fix $\bar{A}$ at 0.06 each time the computed $\bar{A}$ is unrealistically less than 0.06. Such a procedure, however, is not recommended since it may introduce biases. The comparison for the thick cloud case, unlike the ocean and thin cloud cases, yields higher values with the Gautier et al. model. The differences are less than 10 W m^{-2} at 31.5°N but reach over 20 W m^{-2} at the equator during the Northern Hemisphere winter. Since our model is designed for use with monthly, 1000-km-resolution ERB planetary-albedo data, which most likely represent an average of clear-sky, thin-, and thick-cloud conditions, the above results suggest that the discrepancy between the two models might be reduced at those spatial and temporal scales. One should emphasize, however, the qualitative character of the above analysis. Our only objectives in this section are to produce an estimate of the order of magnitude of the discrepancies and to provide a framework from which to estimate the accuracy of the method introduced here.

4. Discussion and conclusions

In (17), it is assumed that (1), which is valid instantaneously, can be applied to monthly time scales as well. To assess the validity of this assumption, we compared surface solar irradiance computed on an

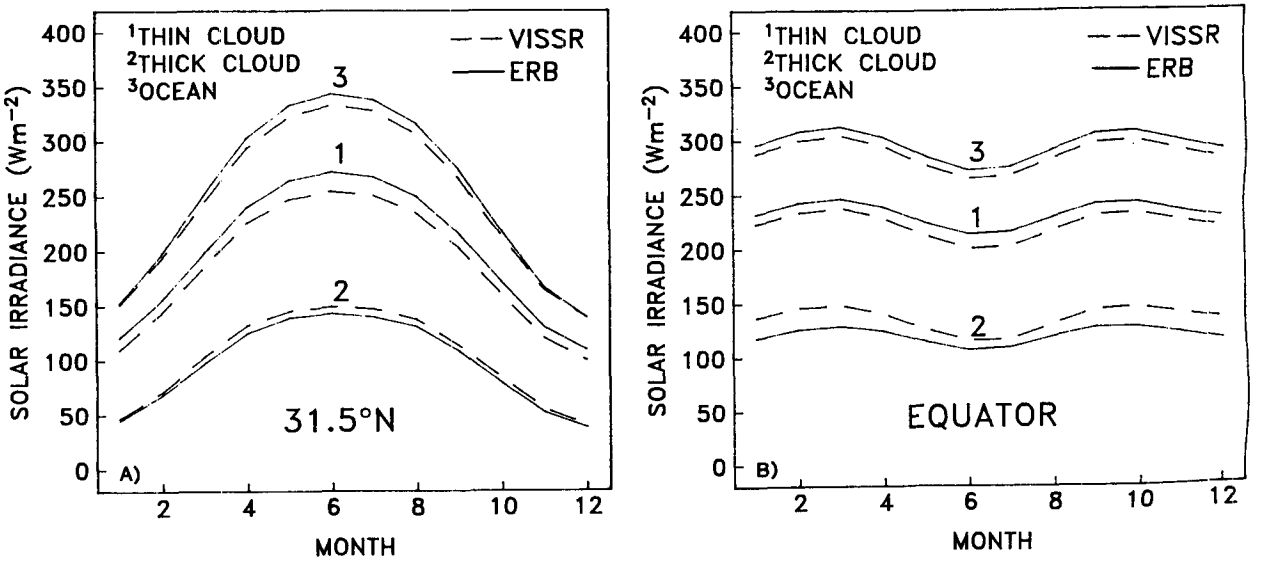

FIG. 9. Monthly net surface solar irradiance at (a) 31.5°N (b) and the equator computed using the ERB-based model and the Gautier et al. (1980) model.

hourly basis and then processed into monthly averages with surface solar irradiance computed as the product of the monthly averaged clear-sky value and the monthly average of instantaneous cloud factors. In the calculations, the method of Gautier et al. (1980) was applied to *GOES-6* VISSR data acquired over the central equatorial Pacific. The results, displayed in Fig. 10 for March 1984, show that the two types of estimates are in close agreement, the rms difference not exceeding a few watts per square meter and the bias being negligible.

Another model assumption requiring discussion is that $\bar{A}_s$ is fixed 0.06 for all latitudes and months. Budyko (1963) and Payne (1972) have shown that $\bar{A}_s$ reaches significantly higher values at high latitudes, especially in winter when the sun remains low above the horizon. At 60°N in January, for instance, $\bar{A}_s = 0.28$ according to Payne (1972). This, however, should not be a problem since $\bar{\alpha}$ and, hence, $\bar{\alpha}\bar{A}_s$ in (20) is small at high latitudes during winter.

The present model has some similarities with the one introduced by Dedieu et al. (1987). In both approaches, the effects due to the clear atmosphere and those due to clouds are decoupled, and satellite-based planetary-albedo information is used to estimate surface solar irradiance. However, the model of Dedieu et al. is significantly different from the new model in ways that make it more difficult to use the earlier model for global applications. Dedieu et al. assigned constant values to the atmospheric content of water vapor and ozone and neglect cloud absorption, whereas these quantities vary as a function of latitude and season in the present treatment. Changes in water vapor and ozone amounts, however, could easily be introduced in the Dedieu et al. model. More importantly, the earlier model was designed to incorporate spectral-radiance data that must be converted to broadband albedo, a nontrivial task. In addition, the technique of Dedieu et al. was designed explicitly for high-resolution (2.5-km) Meteosat data. To use it to process a large-scale, long-term database would be prohibitively expensive, requiring massive computer resources over an extended period. In contrast, the present approach economically provides a global-scale, long-term database. The drawback, however, is the 1000-km spatial resolution of the ERB wide-field-of-view radiometer, which obviously will not allow the effect of smaller-scale features such as the intertropical convergence zone (ITCZ) to be resolved adequately.

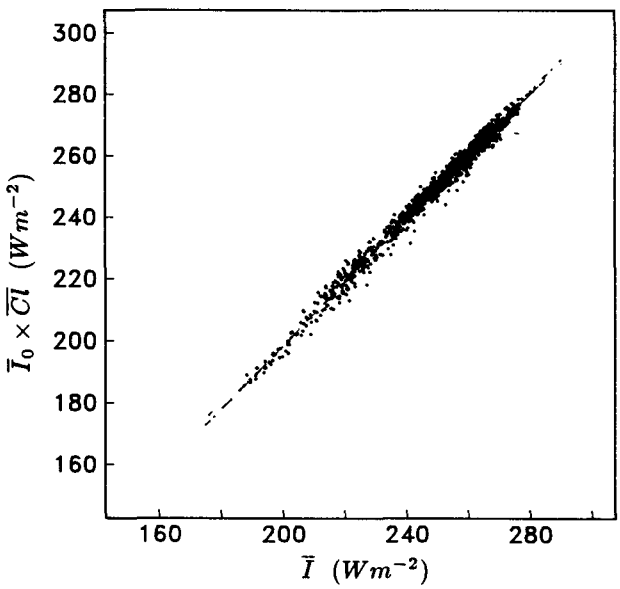

FIG. 10. Scatterplot that validates the computation of monthly averaged surface solar irradiance as the product of a monthly averaged clear-sky value $\bar{I}_0$ and a monthly averaged cloud factor $\overline{Cl}$. Monthly averaged surface solar irradiance, obtained using two different methods, are compared for a 160-km × 160-km grid in the central equatorial Pacific. In the first method, surface solar irradiance is computed from ten instantaneous GOES VISSR observations per day and then processed into monthly averages, while in the second procedure monthly averaged surface solar irradiance is computed as the product of the monthly clear-sky value $\bar{I}_0$ and a monthly averaged cloud factor, $\overline{Cl}$ (the average of all instantaneous cloud factors). The surface solar irradiance is computed according to Gautier et al. (1980).

The development of the new solar-irradiance model provides a major advance in climate-monitoring capabilities. It was made possible by recent advances in basic research in remote sensing (e.g., Tanré et al. 1979; Gautier et al. 1980; Dedieu et al. 1987; Frouin et al. 1989), together with the availability of reliable radiative transfer codes, represented here by the 5S code. Although the new model has not been verified in the present study, it has been compared theoretically with the Gautier et al. model. The results have shown that the two models generally agree to within 10–20 W m^{-2}, as our model yields higher estimates than the Gautier et al. model in clear and thin-cloud conditions and lower estimates in thick-cloud conditions.

Test calculations using actual satellite data to validate the general approach and this model in particular are now necessary. Therefore, in the second part of this set [i.e., Chertock et al. (1992), as well as in Chertock (1989)], values generated using this technique are compared with corresponding values obtained using other satellite techniques. These investigations also include comparisons with long-term climatologies based on ship observations and empirical formulas, and discussions of potential research applications for the new database.

Acknowledgments. Part of the research presented here is from Chertock (1989), the doctoral dissertation of Beth Chertock. During her graduate studies, Dr. Chertock benefited from two major sources of financial support: a National Science Foundation Graduate Fellowship and a National Aeronautics and Space Administration Graduate Student Researcher Program Fellowship. In addition, this work was supported in part by the National Aeronautics and Space Admin-

istration (Grants G-NASA-NAG5-236 and NGT-50057), the National Oceanic and Atmospheric Administration (Grant NA86AA-D-AC051), the National Science Foundation (Grant ATM84-13953), and the California Space Institute (Grant CS81-85). Computer resources were supplied by the Climate Research Division and the California Space Institute at Scripps Institution of Oceanography, and the Wave Propagation Laboratory of the National Oceanic and Atmospheric Administration. The authors thank Dr. Pierre-Yves Deschamps, University of Lille, France, for helpful comments.

REFERENCES

Bates, J., and C. Gautier, 1989: Interaction between net shortwave flux and sea surface temperature. *J. Appl. Meteor.*, **28,** 43–51.

Budyko, M. I., Ed., 1963: Atlas Teplovogo Balansa Zemnogo Shara (Atlas of the Heat Balance of the Earth). Gidrometeoizdat, [Also, Guide to the Atlas of the Heat Balance of the Earth. Translated by I. A. Donehoo, U.S. Weather Bureau, WB/T-106, Washington, D.C.]

Cess, R. L., and I. L. Vulis, 1989: Inferring surface solar absorption from broadband satellite measurements. *J. Climate,* **2,** 974–985.

Chertock, B., 1989: Global monitoring of net solar irradiance at the ocean surface using Nimbus-7 satellite data. Doctoral dissertation, Scripps Institution of Oceanography, University of California, San Diego, 118 pp.

——, R. Frouin, and C. Gautier, 1992: A technique for global monitoring of net solar irradiance at the ocean surface. Part II: Validation. *J. Appl. Meteor.*, **31,** 1067–1083.

Darnell, W. L., W. F. Staylor, S. K. Gupta, and F. M. Denn, 1988: Estimation of surface insolation using sun-synchronous satellite data. *J. Climate,* **1,** 820–835.

Dedieu, G., P. Y. Deschamps, and Y. H. Kerr, 1987: Satellite estimation of solar irradiance at the surface of the earth and of albedo using a physical model applied to Meteosat data. *J. Climate Appl. Meteor.*, **26,** 79–87.

Ellis, J. S., and T. H. Vonder Haar, 1979: Solar radiation reaching the ground determined from meteorological satellite data. Final Rep. NASA Grant NAS5-22372, 68 pp. [NTIS N79-27770-3GA.]

Foot, J. S., 1988: Some observations of the optical properties of clouds. I. Stratocumulus. *Quart. J. Roy. Meteor. Soc.*, **114,** 129–144.

Frouin, R., C. Gautier, K. B. Katsaros, R. J. Lind, 1988: A comparison of satellite and empirical formula techniques for estimating insolation over the oceans. *J. Appl. Meteor.*, **27,** 1016–1023.

——, D. W. Lingner, C. Gautier, K. Baker, and R. Smith, 1989: A simple analytical formula to compute clear sky total and photosynthetically available solar irradiance at the ocean surface. *J. Geophys. Res.*, **94,** 9731–9742.

Gautier, C., 1981: Daily shortwave energy budget over the ocean from geostationary satellite measurements. *Oceanography from Space,* J. R. F. Gowen, Ed., Plenum Press, 201–206.

——, 1988: Surface solar irradiance in the central Pacific during Tropic Heat: Comparisons between in situ measurements and satellite estimates. *J. Climate,* **1,** 600–608.

——, and K. B. Katsaros, 1984: Insolation during STREX: 1. Comparison between surface measurements and satellite estimates. *J. Geophys. Res.*, **89,** 11 779–11 788.

——, G. Diak, and S. Masse, 1980: A simple physical model to estimate incident solar radiation at the surface from GOES satellite data. *J. Climate Appl. Meteor.*, **19,** 1005–1012.

Goody, R. M., 1964: Atmospheric Radiation 1, Theoretical Basis. Oxford University Press, 436 pp.

Hay, J. E., and K. J. Hanson, 1978: A satellite-based methodology for determining solar irradiance at the ocean surface during GATE. *Bull. Amer. Meteor. Soc.*, **59,** 1549.

Justus, C. G., M. V. Paris, and J. D. Tarpley, 1986: Satellite-measured insolation in the United States, Mexico, and South America. *Remote Sens. Environ.*, **20,** 57–83.

Malkmus, W., 1967: Random Lorentz band model with exponential-tailed S^{-1} line-intensity distribution function. *J. Opt. Soc. Am.*, **57,** 323–329.

McClatchey, R. A., R. W. Fenn, J. E. A. Selby, F. E. Voltz, and J. S. Garing, 1971: Optical properties of the atmosphere. AFCRL 71-0279, Environmental Research Paper 354, 108 pp.

Minnis, P., and E. F. Harrison, 1984: Diurnal variability of regional cloud and clear-sky radiative parameters derived from GOES data. Part III: November 1978 radiative parameters. *J. Climate Appl. Meteor.*, **23,** 1032–1051.

Moser, W., and E. Raschke, 1984: Incident solar radiation over Europe estimated from Meteosat data. *J. Climate Appl. Meteor.*, **23,** 166–170.

Payne, R. E., 1972: Albedo of the sea surface. *J. Atmos. Sci.*, **29,** 959–970.

Pinker, R. T., and J. A. Ewing, 1985: Modeling surface solar radiation: Model formulation and validation. *J. Climate Appl. Meteor.*, **24,** 389–401.

Ramanathan, V., 1986: Scientific use of surface radiation budget data for climate studies. Surface Radiation Budget for Climate Applications, J. T. Suttles and G. Ohring, Eds., NASA Ref. Publ. 1169, 58–86.

Raphael, C., and J. Hay, 1984: An assessment of models which use satellite data to estimate solar irradiance at the earth's surface. *J. Climate Appl. Meteor.*, **23,** 832–844.

Raschke, E., T. H. Vonder Haar, W. R. Bandeen, and M. Pasternak, 1973: The annual radiation balance of the earth–atmosphere system during 1969–70 from Nimbus 3 measurements. *J. Atmos. Sci.*, **30,** 341–364.

Smith, W. L., L. D. Herman, T. Schreiner, H. B. Howell, and P. Menzel, 1981: Radiation budget characteristics of the onset of the summer monsoon. *Proc. Int. Conf. on Early Results of FGGE and Large-Scale Aspects of its Monsoon Experiments.* Tallahassee, WMO, 6-16–6-26.

Stephens, G. L., Ackerman, S., and E. A. Smith, 1984: A shortwave parameterization revised to improve cloud absorption. *J. Atmos. Sci.*, **41,** 687–690.

Tanré, D., P. Y. Deschamps, and A. de Leffe, 1979: Atmospheric modeling for space measurements of ground reflectances, including bidirectional properties. *Appl. Opt.*, **18,** 3587–3594.

——, C. Deroo, P. Duhaut, M. Herman, J. J. Morcrette, J. Perbos, and P. Y. Deschamps, 1986: Simulation of the satellite signal in the solar spectrum (5S) model user's guide, 259 pp. [Available from Laboratoire d'Optique Atmosphérique, Université des Sciences et Techniques de Lille, 59655 Villeneuve d'Ascq Cedex, France.]

Tarpley, J. D., 1979: Estimating incident solar radiation at the surface from geostationary satellite data. *J. Climate Appl. Meteor.*, **18,** 1172–1181.

Taylor, V. R., and L. L. Stowe, 1984: Reflectance characteristics of uniform earth and cloud surfaces derived from NIMBUS-7 ERB. *J. Geophys. Res.*, **89,** 4987–4996.

World Meteorological Organization, 1983: Rep. of WMO (CAS)/Radiation Commission of IAMAP meeting of experts on aerosols and their climatic effects. WCP-55, World Meteorological Organization, Geneva.